12-2019

An algorithm for coupling multibranch in vitro experiment to numerical physiology simulation for a hybrid cardiovascular model

Ehsan Mirzaei

Masoud Farahmand

Ethan Kung

An Algorithm for Coupling Multi-Branch In-vitro Experiment to Numerical Physiology Simulation for a Hybrid Cardiovascular Model

Short Title: Algorithm for Hybrid Cardiovascular Model Coupling

Ehsan Mirzaei[1], Masoud Farahmand[1], Ethan Kung[1,2,*]

[1]*Department of Mechanical Engineering, Clemson University, Clemson, SC, USA*

[2]*Department of Bioengineering, Clemson University, Clemson, SC, USA*

Keywords: iterative; mock circuit; lumped-parameter; Broyden's method; hybrid framework; medical device testing;

***Correspondence to:** Ethan Kung, Department of Mechanical Engineering, Clemson University, Fluor Daniel Engineering Innovation Building, Clemson, SC, 29634, USA

Email: ekung@clemson.edu

Citation:

Mirzaei, E, Farahmand, M, Kung, E. An algorithm for coupling multibranch in vitro experiment to numerical physiology simulation for a hybrid cardiovascular model. *Int J Numer Meth Biomed Engng*. 2019;e3289. https://doi.org/10.1002/cnm.3289

Abstract

The hybrid cardiovascular modeling approach integrates an in-vitro experiment with a computational lumped-parameter simulation, enabling direct physical testing of medical devices in the context of closed-loop physiology. The interface between the in-vitro and computational domains is essential for properly capturing the dynamic interactions of the two. To this end, we developed an iterative algorithm capable of coupling an in-vitro experiment containing multiple branches to a lumped-parameter physiology simulation. This algorithm identifies the unique flow waveform solution for each branch of the experiment using an iterative Broyden's approach. For the purpose of algorithm testing, we first used mathematical surrogates to represent the in-vitro experiments and demonstrated five scenarios where the in-vitro surrogates are coupled to the computational physiology of a Fontan patient. This testing approach allows validation of the coupling result accuracy as the mathematical surrogates can be directly integrated into the computational simulation to obtain the "true solution" of the coupled system. Our algorithm successfully identified the solution flow waveforms in all test scenarios with results matching the true solutions with high accuracy. In all test cases, the number of iterations to achieve the desired convergence criteria was less than 130. To emulate realistic in-vitro experiments in which noise contaminates the measurements, we perturbed the surrogate models by adding random noise. The convergence tolerance achievable with the coupling algorithm remained below the magnitudes of the added noise in all cases. Finally, we used this algorithm to couple a physical experiment to the computational physiology model to demonstrate its real-world applicability.

1. Introduction

Both numerical and experimental approaches have been widely used to model the cardiovascular system and medical devices [1–4], albeit each with its own challenges. Numerical simulation of closed-loop physiology coupled to geometries with large deformations is still a difficult task; studies involving hemodynamic simulations of devices with moving parts and fluid-structure interactions have mainly prescribed fixed boundary conditions [5,6]. In-vitro studies, on the other hand, provide the possibility of direct pressure and flow measurements to capture complex fluid phenomena [7–10]; however, they suffer from the excessive number of components and connections required to build an intricate vascular model as well as difficulties in accurately reproducing closed-loop cardiac response such as preload sensitivities [11–14]. The current method of utilizing experimental data in reduced order models is largely for the purpose of model parameter estimation [15].

A hybrid framework can leverage the strengths of both experimental and numerical approaches by coupling an in-vitro experiment to a lumped-parameter network (LPN) simulation of cardiovascular physiology. LPN models consisting of elements such as resistance, capacitance, inductance, diode and a heart model offer a simplified 0-D approach for simulating the cardiovascular system. In-vitro experiments, on the other hand, can directly contain medical devices and physical components mimicking cardiovascular mechanics. In a hybrid framework, the in-vitro experiment operates in a dynamically changing feedback environment with the LPN simulation, allowing for the simultaneous investigation of the behavior of the physical components in the experiment and the corresponding impacts in the simulated physiology.

The hardware-in-loop (HIL) technique is a method that has been used to construct cardiovascular hybrid frameworks[16–18]. However, the real-time nature of previous implementations results in constraints by signal noise and bandwidth of the hydraulic sensors and actuators, limiting the final model accuracy. These limitations motivate the development of a more robust technique for performing HIL in a hybrid framework.

To this end, we have previously introduced the Physiology Simulation Coupled Experiment framework [19] and demonstrated the coupling of a 2-branch (one inlet and one outlet) in-vitro experiment to an LPN physiology simulation using a proportional-control-based coupling algorithm. In the present study, we introduce a Broyden-method-based algorithm capable of integrating a multi-branch (i.e. more than two branches) experiment with a computational physiology simulation, enabling the closed-loop coupling of the two. The goal of this work is to provide a tool for interfacing the two domains, therefore the qualities of the physical experiment and the physiology simulation components themselves remain the responsibility of the user of this tool.

2. Methods

In this study, we use a numerical model of the Fontan physiology as the computational domain for demonstrating the operation of the coupling algorithm. This model has been verified against clinical data and explained in details in our previous study [20]. The LPN has been constructed such that the pressure produced by the single ventricle heart block drivers the flow through the pulmonary and systemic circuits. The LPN parameters related to cardiac function and vascular resistances and compliances are adjusted according to a patient body size and exercise intensity. The closed-loop LPN realistically models the physiological parameters of a Fontan patient. The data from the in-vitro experiment include pressure and flow measurements. For a closed-loop coupling of an experimental section to a physiology simulation to occur, flow and

pressure data should be interactively communicated between the two domains. The coupling algorithm functions as an interface providing the boundary conditions for each domain to create a coupled system; it is important to note that this process does not influence the LPN parameters.

This section begins by introducing the mathematical formulation of the coupling problem, followed by the discussion of the iterative procedure used for identifying the solution waveforms. Next, we provide an overview of the Broyden's method including justification for its use in the algorithm. Finally, we propose a technique for improving convergence stability and present results quantifying the accuracy of the algorithm and its robustness against measurement noise.

To illustrate the concept of the multi-branch coupling approach, we consider a rigid, 3-branch (two inlets, one outlet) experimental section coupled to an LPN model of a Fontan patient obtained from our previous work [20] (Figure 1). For each branch of the experimental section there exists a unique flow waveform that results in the same pressure change from the inlet to the outlet in both the experimental and numerical models; this is the solution flow waveform. The aim is to identify these solution waveforms in order to achieve a coupled system.

In Figure 1, a flow waveform (Q_1) applied to inlet 1 in both the experimental and numerical models gives rise to pressure changes of ΔP_{Exp1} and ΔP_{LPN1} respectively. ΔP_{Exp1} is the resulting pressure change from inlet 1 to outlet 3 in the experimental section while ΔP_{LPN1} is the corresponding pressure change between points 1 and 3 in the LPN. The same holds true for the second inlet. Subsequently, we define an error function for every inlet by subtracting the associated pressure changes from each domain. For the scenario in Figure 1, the set of error functions is defined as:

$$\begin{cases} E_1(Q_1, Q_2) = \Delta P_{LPN1} - \Delta P_{Exp1} & for\ inlet\ 1 \\ E_2(Q_1, Q_2) = \Delta P_{LPN2} - \Delta P_{Exp2} & for\ inlet\ 2 \end{cases} \quad (1)$$

Due to mass conservation in the experimental section, the outlet flow (Q_3) is the sum of two inlet flows, i.e. $Q_3 = Q_1 + Q_2$. As a result, we have a system of two nonlinear equations in two variables, where each variable is a flow waveform represented by a vector of flow values. Solving this set of equations simultaneously, i.e. finding their roots, provides the solution flow waveforms that generate identical pressure changes in the physical and numerical domains, i.e. $\Delta P_{LPN1} = \Delta P_{Exp1}$ for inlet 1 and $\Delta P_{LPN2} = \Delta P_{Exp2}$ for inlet 2. This creates a closed-loop coupling between the experimental section and the LPN model.

We derived an iterative procedure for solving the set of error functions and identifying the solution flow waveforms (Figure 2). An initial guess flow waveform is prescribed to every branch of the experimental section and numerical physiology simulation and the resulting pressure changes from each domain are compared to obtain the error waveforms as described by Eq. 1. Then, Broyden's method, a quasi-Newton method, is employed to update the flow waveforms for the next iteration.

Broyden's method, utilized here for finding the roots of the error functions, is a variant of Newton's method, which is a powerful and widely used technique for solving nonlinear equations. Newton's method takes advantage of Taylor series expansion to obtain a linear approximation of the nonlinear function at the point of interest and uses the root of this linear approximation as the next iterate. Although Newton's method converges quadratically, it requires calculating derivatives of the nonlinear functions to form the Jacobian matrix. In our application, the error function values are obtained by subtracting the pressure waveforms that consist of experimental data points, thus not having analytic form. This necessitates the use of finite differences to

numerically approximate the Jacobian in Newton's method, requiring a large number of function evaluations. To avoid this, quasi-Newton methods can be used, the most well-known of which is Broyden's method. In Broyden's update, the Jacobian is replaced by an approximation matrix updated at each iteration by adding a low-rank matrix [21]. As a result, the need for derivative calculation is eliminated. For the problem at hand, therefore, we employ Broyden's method in a way similar to the work of Malossi et al. [22] to minimize the number of function evaluations and experimental runs required.

In Broyden's method, the system of nonlinear error functions, derivatives of which are not analytically available, are solved by applying the following procedure [23]:

$$
\begin{aligned}
&\boldsymbol{Do\ for\ i = 0, 1, \ldots} \\
&\quad \boldsymbol{Solve}\ A^i\, \boldsymbol{s}^i = -\boldsymbol{E}(\boldsymbol{Q}^i)\ for\ \boldsymbol{s}^i \qquad where\ \boldsymbol{Q} = \begin{bmatrix} Q_1 \\ Q_2 \\ \vdots \end{bmatrix}\ \&\ \boldsymbol{E}(\boldsymbol{Q}) = \begin{bmatrix} E_1 \\ E_2 \\ \vdots \end{bmatrix} \\
&\quad\ \boldsymbol{Q}^{i+1} := \boldsymbol{Q}^i + \boldsymbol{s}^i \\
&\quad\ \boldsymbol{y}^{i+1} := \boldsymbol{E}(\boldsymbol{Q}^{i+1}) - \boldsymbol{E}(\boldsymbol{Q}^i) \\
&\quad\ A^{i+1} := A^i + \lambda\, \frac{(\boldsymbol{y}^i - A^i \boldsymbol{s}^i)\boldsymbol{s}^{i^T}}{\boldsymbol{s}^{i^T} \boldsymbol{s}^i} \qquad where\ 0 < \lambda \leq 1
\end{aligned}
\tag{1}
$$

where $Q_1, Q_2, \ldots$ are the flow waveforms, each corresponding to one branch of the experimental section, and A is the Jacobian replacement known as the approximation matrix. A value of 0.01 is used for coefficient λ to reduce the occurrence of singularity in A matrices and maintain the smoothness of the flow waveforms during the iterative procedure. Assuming that each flow waveform consists of *N* discrete data points, the algorithm solves *N* distinct sets of error functions. In other words, at each iteration of the algorithm, the flow values for all flow waveforms, i.e. $Q_1, Q_2, \ldots$, at time step t_i are updated together, independent of other time steps. For example, for the 3-branch coupling case in Figure 1, a set of two error functions is solved for each time point of the flow waveforms. For this set of the error functions, there is an associated approximation matrix with a dimension of 2×2. The number of approximation matrices updated at each iteration is equal to the number of time points on each of the flow waveforms.

Finite difference estimates of the Jacobian matrices calculated in the first iteration using the initial values for $\boldsymbol{Q}$ are chosen as the initial approximation matrices, i.e. $A^0 = J(\boldsymbol{Q}^0)$ [23,24]. Over the succeeding iterations, these matrices are updated using Broyden's update described above (Eq. 2), and the algorithm continues until the residual for each branch defined as follows drops below the desired value (chosen to be 0.01 mmHg for algorithm validation and 0.05 mmHg for noise investigation in this study).

$$
Residual_i = \sqrt{\frac{\sum_{j=1}^{N} (E_i[j])^2}{N}} \tag{2}
$$

where *N* is the number of points in the waveform, and *i* indicates the i^{th} branch.

A major drawback of Newton-like methods such as Broyden's is that their convergence is not guaranteed unless the initial guess is sufficiently close to the solution and the Jacobian matrix is nonsingular. To ensure that the algorithm progresses towards the solution, determinants of the approximation matrices are calculated at each iteration to detect matrices with near-zero determinants (nearly singular matrices). If the approximation matrices become nearly singular, the

linear system $A^i\ \boldsymbol{s}^i = -\boldsymbol{E}(\boldsymbol{Q}^i)$ cannot be properly solved to determine $\boldsymbol{s}^i$. As a result, a spike will occur in the waveforms at the corresponding point for the next iteration, preventing the algorithm from converging to the solution. A mediation to this issue involves perturbing the ill-conditioned matrix A^i so that it becomes well-conditioned and then proceeding with the iteration [23]. To do so, we replace the ill-conditioned approximation matrix with the finite difference Jacobian matrix calculated in the first iteration added with an identity matrix [25]. This procedure mitigates the occurrence of singularities, facilitating algorithm convergence.

2.1. Algorithm testing using virtual experiments

For the purpose of testing the coupling algorithm, we use mathematical surrogates to represent the experimental section, referring to these surrogates as "virtual experiments". The rationale for using the virtual experiments is that they can be directly integrated into the LPN to produce reference data (i.e. the actual model solution) for validating the coupling algorithm. Various combinations of HeartWare continuous flow ventricular assist device (VAD), stenosis modeled as a quadratic resistance, and linear resistance are used as virtual experiment elements. The hemodynamic quantity available from the (virtual or physical) experimental element is the pressure difference across the element at a given flow rate. The following relationships define the pressure change across the virtual experiment components used in this study:

$$\begin{aligned} \Delta P &= AQ^2 + BQ + C && \textit{Continuous flow VAD} \\ \Delta P &= kQ^2 && \textit{Stenosis} \\ \Delta P &= RQ && \textit{Linear resistance} \end{aligned} \tag{3}$$

The performance curves of HeartWare describing the pressure increase produced by the VAD (ΔP) based on the flow (Q) passing through it at various rotation speeds are obtained from [26]. A, B and C are coefficients determined experimentally during pump characterization [19,27]. The pressure drop across a stenosis can be modeled as a quadratic function of flow [9,19]. We used a pressure drop coefficient of k = 0.0004 mmHg s^2 ml^{-2} to emulate realistic pressure drops across a vascular stenosis. Linear resistances are utilized to model pressure loss through blood vessels, which is linearly proportional to the flow rate (Q). The values of these constants used in each virtual experiment are listed in Table 1.

The virtual experiments are coupled to the numerical physiology simulation of a single-ventricle circulation representing a patient with a weight and height of 50 kg and 150 cm, respectively, at resting condition [20]. We used a generic sinusoidal waveform as the initial guess of all flow waveforms. We tested five scenarios of virtual experiments, three on the venous side and two on the arterial side of the Fontan physiology simulation, to demonstrate the capability of the algorithm to identify solution waveforms of different amplitudes and shapes. On the venous side, two, three and four branch sections (Figure 3), and on the arterial side, two and three branch sections (Figure 4) are coupled to the LPN model.

More specifically, on the venous side, for the 2-branch coupling case, a HeartWare VAD is coupled to the inferior vena cava of the Fontan LPN. In the 3-branch scenario, the virtual experiment consists of a stenosis at inlet 1 and a HeartWare VAD at inlet 2. Finally, the 4-branch virtual experiment includes a linear resistance at inlet 1, a HeartWare VAD at inlet 2, a pulmonary artery stenosis together with a linear resistance at outlet 3 and a linear resistance at outlet 4 (Figure 3). Two scenarios are considered for the arterial side. The 2-branch case comprises a HeartWare

VAD connected between the ventricle and aorta, while the 3-branch scenario involves a stenosis representing an aortic coarctation at the inlet of the virtual experiment and a pair of a linear resistance and an inductor at both outlets (Figure 4).

To study the relationship between the pressure change across a branch in the experimental section and the number of iterations required to achieve convergence, we also examined different values of the stenosis coefficient (Table 2) placed at inlet 1 of the venous side 3-branch coupling case (Figure 3 B). A higher value of *k* corresponds to a larger pressure drop across the stenosis.

To validate the accuracy of the coupling results, the equations describing the virtual experiments were integrated directly with the LPN into a monolithic simulation to acquire the "true solutions" for comparison against the solutions obtained by the coupling algorithm. We use normalized root mean square error (NRMSE) as defined in Eq. 5 below to measure the quality of fit between the coupling and validation waveforms represented by x_1 and x_2, respectively:

$$NRMSE(x_1, x_2) = \frac{RMSE(x_1, x_2)}{\max(x_2) - \min(x_2)} \quad (4)$$

The virtual experiments used in this study do not reflect the noisy nature of in-vitro experiments. To examine the robustness of the algorithm against uncertainty in the experimental measurements, we modified the pressure change waveforms in all test cases. At each iteration of the algorithm, we added a random number chosen from uniformly distributed values in the range of [0, 0.1] to the amplitudes of the five lowest frequencies of the pressure change waveforms for every branch of the virtual experiments. This resulted in up to 0.9 mmHg RMSE variation in the pressure change waveforms (Table 3), mimicking realistic in-vitro measurements. To accommodate for the added noise, we used a convergence tolerance of 0.05 mmHg for these tests.

2.2. Demonstration of coupling algorithm applied to a physical experiment

We applied the coupling algorithm to couple a physical experiment to the Fontan LPN using a convergence criterion of 0.1mmHg. The experimental section contained an 85% Inferior Vena Cava (IVC) stenosis phantom model with a circular cross section diameter of 19mm (Figure 5A). The phantom was constructed using a high resolution 3D-printer (Connex 350 Polyjet, Stratasys Inc.) and rigid material (VeroClear, Stratasys Inc.). A computer programmable pump capable of producing precise pulsatile flow waveforms created the flow through the phantom (Figure 5C). The working fluid was a 40%-glycerol solution with a density (1092 $kg.m^{-3}$) and a dynamic viscosity (41×10-4 Pa.s) similar to those of the human blood. Two catheter pressure sensors (PEC10C&D, Miller Instruments) connected to a pressure box (PCU 2000, Miller Instruments) were installed at the inlet and outlet of the phantom, to monitor the pulsatile pressure waveforms. To record the volumetric flow rate a flow probe (16PXL, Transonic Systems) connected to a flow meter (TS410, Transonic Systems) was mounted on a Tygon tubing downstream of the experimental section as shown in schematic Figure 6. A custom Matlab program interfaced via separate National Instrument modules (NI 9205 and NI 9263, National Instruments) mounted on a single DAQ chassis (NI cDAQ 9174, National Instruments) were used to control the programmable pump and collect pressure and flow signals at a sampling rate of 1000Hz. Similar to our earlier work [19], we improved the signal to noise ratio by averaging 20 cycles of each data acquisition and then using a fourth-order low-pass Butterworth filter set at 20Hz to remove the high-frequency components. The initial flow for starting the coupling

algorithm is chosen to be the IVC flow as simulated by the Fontan LPN alone without the IVC stenosis.

3. Results

3.1. Algorithm testing using virtual experiments

The venous side coupling cases produced excellent agreements between the waveforms obtained from the coupling algorithm and of the true solutions with NRMSE values ranging between 0.269% ~ 0.855% (Figure 7). Similarly, the small NRMSE (0.378% ~ 0.854%) values for the arterial side coupling results demonstrate the accuracy of the algorithm under more pulsatile flow conditions (Figure 8).

We observed that the rate of residual decrease for each branch is proportional to the amount of pressure change across the branch; the larger the pressure change, the faster the residual decreased for the corresponding branch. For example, in the case of 3-branch coupling on the venous side (Figure 3 B), the very small pressure drop across inlet 1 resulted in a slower residual decrease rate compared to inlet 2 which had a significantly higher pressure change (Figure 9 A). On the other hand, for the arterial side 3-branch case (Figure 4 B), the ratio between pressure drops across outlets 1 and 2 was remarkably lower than that for the venous side 3-branch case; therefore, the residuals decrease at approximately the same rate (Figure 9 B). In addition, increasing the pressure drop across the stenosis at inlet 1 of the venous side 3-branch case (Figure 3 B) by using larger pressure drop coefficients resulted in significantly faster convergence (Table 2), corroborating the finding that larger pressure change leads to faster convergence rates.

Finally, the number of iterations for all test cases, with and without noise, was in the range of 10 ~ 126 (Table 3). At equal convergence tolerance, the added noise increased the number of iterations required for all scenarios except for the scenario of the venous side 2-branch coupling (Table 3). We also note that the achievable convergence tolerance (0.05 mmHg) was smaller than the maximum amplitude of noise added to the pressure change waveforms, which was in the range of 0.175 ~ 0.894 mmHg RMSE.

3.2. Demonstration of coupling algorithm applied to a physical experiment

The flow solution of the final (30^{th}) iteration revealed a significant effect of the IVC stenosis on the IVC flow waveform (Figure 10 A). Overall, the average IVC flow in presence of the stenosis decreased by 10% and the solution of the algorithm converged to a residual of 0.04mmHg (97% decrease in the residual) within 30 iterations (Figure 10 B). In general, each algorithm iteration required 6~10 minutes of experimental run time; the total run time of the hybrid model was 214 minutes.

4. Discussion

The choice of the initial guess has a significant impact on the convergence of the Broyden's method; the closer the initial guess is to the solution, the fewer iterations are required to identify the solution [23,28,29]. In other words, a strategic initial guess can improve the convergence of the algorithm. This idea is clear from examining the convergence behavior in Fig 10B; if the flow

waveform of iteration 10 with a residual of ~0.6mmHg is used as the initial guess instead, the algorithm would take merely 20 iterations to converge instead of 30. To demonstrate the robustness of our algorithm, we used a generic sinusoidal waveform as the initial guess in all test cases. Despite starting from this generic initial guess, the algorithm successfully converged in less than 130 iterations for all test cases. In the practical usage of this algorithm to couple an actual experiment to a numerical physiology simulation, an approximate mathematical surrogate of the in-vitro experiment can be obtained by applying various flows and measuring the corresponding pressure changes. Combining the surrogate with the LPN can provide a better initial guess for the algorithm.

There are a number of alternative techniques for improving the convergence stability of the coupling algorithm other than the one implemented in this study. One alternative approach is the stationary Newton's method [28] in which the initial finite difference approximations of the Jacobian matrices are used for the succeeding iterations without modification, i.e. $A^i = J(\boldsymbol{Q}^0)$ for all $i = 0, 1, 2, 3, etc$. Another approach involves applying appropriate damping coefficients in the range of 0 to 1 while updating the flows and approximation matrices to reduce the step size [28,30]. In this approach, however, determining the appropriate coefficient values for ensuring convergence while minimizing the number of iterations is a challenge. Overall, good choices for initial flows and approximation matrices are crucial to the success of the algorithm. A detailed discussion of the techniques for dealing with convergence properties can be found in [23,28,29,31].

The observation that branches with small pressure changes negatively affect the convergence rate means that in a multi-branch experimental section, the branch with the smallest pressure change determines the overall convergence rate of the hybrid model. For the five scenarios tested in this study, the maximum number of iterations is 126 (Table 3). Considering the typical run time for a physical experiment (6 to 10 minutes), the total time required to identify the solutions in the worst-case scenario does not exceed 24 hours. Compared to the runtime of modern computational fluid dynamic simulations using high-performance computing clusters, which is in the range of few days to few weeks [32,33], the run time of our proposed hybrid model can be considered reasonably practical.

By integrating the virtual experiment directly with the LPN into a monolithic model for coupling results validation, we confirm that the coupled model has a unique, deterministic solution. This is true under the condition that the in-vitro experiment exhibits a consistent behavior, meaning that for a given set of periodic inputs, it produces a fixed set of periodic outputs. If the experiment does not possess a consistent behavior, it may not be possible nor meaningful to identify the coupled solution using an iterative process.

The results from Table 3 suggest that the algorithm is robust against measurement noise. The algorithm is capable of achieving a convergence tolerance below the maximum amplitude of the added noise, suggesting that in an actual application of a hybrid model, this coupling algorithm would not be the limiting factor of the model accuracy.

Application of the algorithm on a physical in-vitro experiment of an IVC stenosis showed that the algorithm was able to capture the interaction between the closed-loop LPN and the in-vitro experiment. The coupling algorithm continuously decreased residual error across the iterations and successfully achieved a convergence tolerance of 0.1mmHg which is equal to the resolution of the pressure sensors.

Limitations: Since the algorithm updates the flow values as well as the approximation matrix associated with a particular time step independent of other time steps, it is not designed to handle

in-vitro models producing a phase shift in the flow and pressure waveforms, for example, a flow conduit with a high inductance value. Compliant elements in an in-vitro experiment exhibiting a time-rate of pressure change linearly proportional to the flow also create a phase shift in the flow and pressure waveforms. Further study is required to identify a new approach for coupling these types of experimental sections to physiology simulations. The algorithm we present here is robust against small phase shifts in the experimental section as demonstrated by the coupling results of the arterial side 3-branch test scenario where inductors with small values are included, as well as its application to the physical experiment where inductances in the flow circuit are present.

5. Conclusion

In this study, we successfully developed an algorithm for coupling an in-vitro experiment containing an arbitrary number of branches to a lumped-parameter physiology simulation. Using Broyden's method, the algorithm solves a set of nonlinear functions to identify the solution flow waveforms, resulting in the closed-loop coupling of the experimental and numerical domains. We utilized a convergence stabilization technique for the algorithm that involves replacement of nearly singular approximation matrices with nonsingular ones. To confirm the accuracy of the algorithm, we coupled mathematical surrogates of five in-vitro experiments to the physiology simulation of a Fontan patient, and verified the coupling results against "true solutions" obtained from integrating the surrogate models directly with the physiology simulation. The coupling results matched the true solutions very closely with NRMSE values ranging between 0.269% ~ 0.855%. In all test cases, the algorithm converged with less than 130 iterations. We also added noise to the pressure waveforms of the surrogate models to mimic the measurement uncertainty in an actual experiment. In all noise-test cases, the algorithm achieved convergence with a tolerance smaller than the maximum amplitude of noise added to the pressure change waveforms. This validated algorithm can be used to couple a range of in-vitro experiments containing multiple branches to physiology simulations. Finally, our demonstration of the coupling algorithm applied to a physical experiment confirmed its real-world usability.

Acknowledgments This work was supported by Clemson University, an award from the American Heart Association and The Children's Heart Foundation (16SDG29850012), and an award from the National Science Foundation (CAREER1749017). The funding sponsors of this work have no involvement in the study design, the collection, analysis and interpretation of data, in the writing of the manuscript, and in the decision to submit the manuscript for publication.

Data Accesssibility The authors are making the data associated with this paper publically available.

References

1. Kung EO, Les AS, Medina F, Wicker RB, McConnell M V, Taylor CA. In Vitro Validation of Finite-Element Model of AAA Hemodynamics Incorporating Realistic Outlet Boundary Conditions. *Journal of Biomechanical Engineering* 2011; **133**(4):041003. doi:10.1115/1.4003526.

2. Taylor CA, Draney MT. Experimental and Computational Methods in Cardiovascular Fluid Mechanics. *Annual Review of Fluid Mechanics* 2004; **36**(1):197–231. doi:10.1146/annurev.fluid.36.050802.121944.

3. Cebral JR, Castro MA, Burgess JE, Pergolizzi RS, Sheridan MJ, Putman CM. Characterization of cerebral aneurysms for assessing risk of rupture by using patient-specific computational hemodynamics models. *American Journal of Neuroradiology* 2005; **26**(10):2550–2559. doi:10.1016/S0098-1672(08)70473-9.

4. Kung EO, Les AS, Figueroa CA, et al. In Vitro Validation of Finite Element Analysis of Blood Flow in Deformable Models. *Annals of Biomedical Engineering* 2011; **39**(7):1947–1960. doi:10.1007/s10439-011-0284-7.

5. Long CC, Marsden AL, Bazilevs Y. Fluid–structure interaction simulation of pulsatile ventricular assist devices. *Computational Mechanics* 2013; **52**(5):971–981. doi:10.1007/s00466-013-0858-3.

6. Marsden AL, Bazilevs Y, Long CC, Behr M. Recent advances in computational methodology for simulation of mechanical circulatory assist devices. *Wiley Interdisciplinary Reviews: Systems Biology and Medicine* 2014; **6**(2):169–188. doi:10.1002/wsbm.1260.

7. Keshavarz-Motamed Z, Garcia J, Maftoon N, Bedard E, Chetaille P, Kadem L. A new approach for the evaluation of the severity of coarctation of the aorta using Doppler velocity index and effective orifice area: In vitro validation and clinical implications. *Journal of Biomechanics* 2012; **45**(7):1239–1245. doi:10.1016/j.jbiomech.2012.01.039.

8. Hang T, Giardini A, Biglino G, Conover T, Figliola RS. In vitro validation of a multiscale patient-specific norwood palliation model. *ASAIO Journal* 2016; **62**(3):317–324. doi:10.1097/MAT.0000000000000336.

9. Ha H, Lantz J, Ziegler M, et al. Estimating the irreversible pressure drop across a stenosis by quantifying turbulence production using 4D Flow MRI. *Scientific Reports* 2017; **7**(November 2016):1–14. doi:10.1038/srep46618.

10. Vukicevic M, Chiulli JA, Conover T, Pennati G, Hsia TY, Figliola RS. Mock circulatory system of the fontan circulation to study respiration effects on venous flow behavior. *ASAIO Journal* 2013; **59**(3):253–260. doi:10.1097/MAT.0b013e318288a2ab.

11. Gregory SDD, Stevens M, Timms D, Pearcy M. Replication of the Frank-Starling response in a mock circulation loop. *Conf Proc IEEE Eng Med Biol Soc* 2011; **2011**:6825–6828. doi:10.1109/IEMBS.2011.6091683.

12. Gwak KW, Paden EB, Noh MD, Antaki JF. Fluidic operational amplifier for mock circulatory systems. *IEEE Transactions on Control Systems Technology* 2006; **14**(4):602–

612. doi:10.1109/TCST.2006.876624.

13. Pantalos GMM, Koenig SCC, Gillars KJJ, Giridharan GAA, Ewert DLL. Characterization of an adult mock circulation for testing cardiac support devices. *ASAIO J* 2004; **50**(1):37–46. doi:10.1097/01.MAT.0000104818.70726.E6.

14. Baloa LA, Boston JR, Antaki JF. Elastance-based control of a mock circulatory system. *Ann Biomed Eng* 2001; **29**(3):244–251.

15. Shi Y, Lawford P, Hose R. Review of Zero-D and 1-D Models of Blood Flow in the Cardiovascular System. *BioMedical Engineering OnLine* 2011; **10**(1):33. doi:10.1186/1475-925X-10-33.

16. Nestler F, Bradley AP, Wilson SJ, Timms DL, Frazier OH, Cohn WE. A hybrid mock circulation loop for a total artificial heart. *Artif Organs* 2014; **38**(9):775–782. doi:10.1111/aor.12380.

17. Darowski M, Kozarski M, Ferrari G, et al. A new hybrid (hydro-numerical) model of the circulatory system. *Bulletin of the Polish Academy of Sciences: Technical Sciences* 2013; **61**(4):993–1003.

18. Ochsner G, Amacher R, Amstutz A, et al. A Novel Interface for Hybrid Mock Circulations to Evaluate Ventricular Assist Devices. 2013; **60**(2):507–516.

19. Kung E, Farahmand M, Gupta A. A Hybrid Experimental-Computational Modeling Framework for Cardiovascular Device Testing. *Journal of Biomechanical Engineering* 2019; **141**(5):051012. doi:10.1115/1.4042665.

20. Kung E, Pennati G, Migliavacca F, et al. A Simulation Protocol for Exercise Physiology in Fontan Patients Using a Closed Loop Lumped-Parameter Model. *Journal of Biomechanical Engineering* 2014; **136**(8):081007. doi:10.1115/1.4027271.

21. Fang H, Saad Y. Two classes of multisecant methods for nonlinear acceleration. *Numerical Linear Algebra with Applications* 2009; **16**(3):197–221. doi:10.1002/nla.617.

22. Malossi ACI, Blanco PJ, Crosetto P, Deparis S, Quarteroni A. Implicit Coupling of One-Dimensional and Three-Dimensional Blood Flow Models with Compliant Vessels. *Multiscale Modeling & Simulation* 2013; **11**(2):474–506. doi:10.1137/120867408.

23. Dennis JE, Schnabel RB. *Numerical Methods for Unconstrained Optimization and Nonlinear Equations*. Society for Industrial and Applied Mathematics; 1996.

24. Kelley CT. *Solving Nonlinear Equations with Newton's Method*. Society for Industrial and Applied Mathematics; 2003.

25. Ortega JM, Rheinboldt WC. *Iterative Solution of Nonlinear Equations in Several Variables*. Society for Industrial and Applied Mathematics; 2000.

26. Schmidt T, Rosenthal D, Reinhartz O, et al. Superior performance of continuous over pulsatile flow ventricular assist devices in the single ventricle circulation: A computational study. *Journal of Biomechanics* 2017; **52**:48–54. doi:10.1016/j.jbiomech.2016.12.003.

27. Farahmand M, Kavarana MN, Kung E. Risks and Benefits of Using a Commercially Available Ventricular Assist Device for Failing Fontan Cavopulmonary Support: A Modeling Investigation. *IEEE Transactions on Biomedical Engineering* 2019:1–1. doi:10.1109/TBME.2019.2911470.

28. Martinez JM. Practical quasi-Newton methods for solving nonlinear systems. *Journal of Computational and Applied Mathematics* 2000; **124**(1–2):97–121. doi:10.1016/S0377-0427(00)00434-9.

29. Nocedal J, Wright SJJ. *Numerical Optimization*. Springer New York; 2006.

30. Dennis, Jr. JE, Moré JJ. Quasi-Newton Methods, Motivation and Theory. *SIAM Review* 1977; **19**(1):46–89. doi:10.1137/1019005.

31. Dennis JE. On the Convergence of Broyden's Method for Nonlinear Systems of Equations. *Mathematics of Computation* 1971; **25**(115):559. doi:10.2307/2005218.

32. van Bakel TMJ, Lau KD, Hirsch-Romano J, Trimarchi S, Dorfman AL, Figueroa CA. Patient-Specific Modeling of Hemodynamics: Supporting Surgical Planning in a Fontan Circulation Correction. *Journal of Cardiovascular Translational Research* 2018; **11**(2):145–155. doi:10.1007/s12265-017-9781-x.

33. Kerckhoffs RCP, Neal ML, Gu Q, Bassingthwaighte JB, Omens JH, McCulloch AD. Coupling of a 3D Finite Element Model of Cardiac Ventricular Mechanics to Lumped Systems Models of the Systemic and Pulmonic Circulation. *Annals of Biomedical Engineering* 2006; **35**(1):1–18. doi:10.1007/s10439-006-9212-7.

Tables and Table Captions

Table 1. Summary of coefficient values for virtual experiment components

Coupling Scenario		HeartWare VAD			k [mmHg s^2 ml^{-2}]	R [mmHg s ml^{-1}]	L [mmHg s^2 ml^{-1}]
		A	B	C			
Venous side coupling	2-branch	-0.0037	0.0186	43.674	0.0004	-	-
	3-branch					-	-
	4-branch					$R_{svc}=5.99\times10^{-2}$ $R_{pa1}=1.51\times10^{-1}$ $R_{pa2}=2.01\times10^{-1}$	-
Arterial side coupling	2- branch	-0.0042	0.0675	122.83	-	-	-
	3- branch	-	-	-	0.0004	$R_{uba}=6.87\times10^{-1}$ $R_{tha}=8.18\times10^{-2}$	$L_{uba}=5.48\times10^{-4}$ $L_{tha}=1.33\times10^{-3}$

Table 2. Comparison of the pressure drop coefficient value, the resulting pressure drop, and number of iterations for the venous side 3-branch scenario

Pressure Drop Coefficient (k)	Inlet 1 Mean Pressure Drop [mmHg]	Inlet 2 Mean Pressure Increase [mmHg]	Number of Iterations
0.0004	0.54	31.44	101
0.004	4.02	31.43	48
0.04	24.17	31.27	15
0.4	63.30	31.01	13

Table 3. Comparison of number of iterations for all test scenarios with and without noise, and the maximum amplitude of added noise

Coupling Scenario		Number of Iterations			Amplitude of Added Noise; Max. RMSE [mmHg]
		Without Noise		With Noise	
		CT* = 0.01	CT = 0.05	CT = 0.05	
Venous side coupling	2-branch	16	10	10	0.175
	3-branch	101	81	96	0.182
	4-branch	86	65	75	0.175
Arterial side coupling	2-branch	27	22	26	0.894
	3-branch	123	97	126	0.356

**CT = Convergence Tolerance [mmHg]*

Ehsan Mirzaei

Figure 1. Conceptual illustration of coupling a 3-branch experimental section to a Fontan lumped model; the boxes in the experimental section represent physical components that produce a pressure change when a flow is prescribed

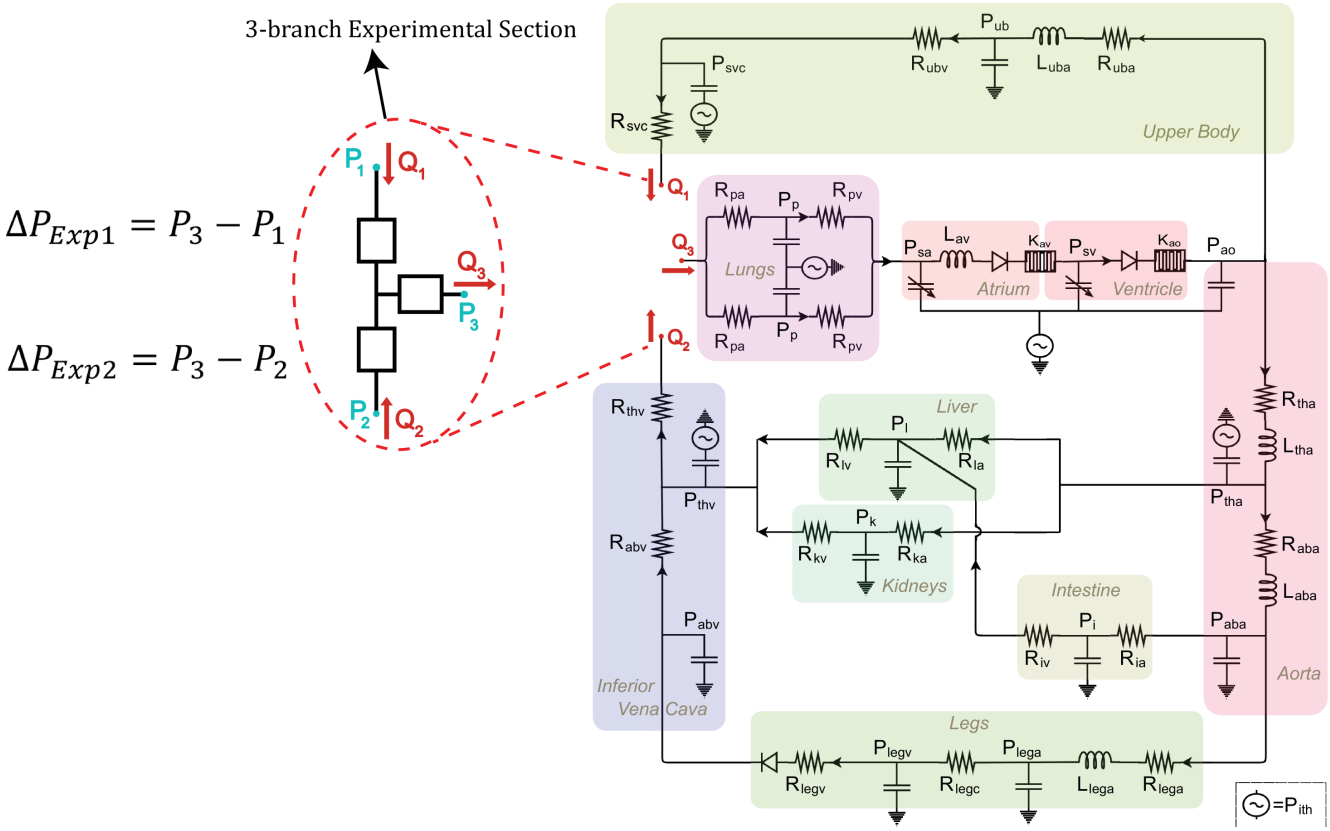

Ehsan Mirzaei

Figure 2. Flowchart of the iterative procedure for identifying the solution waveforms

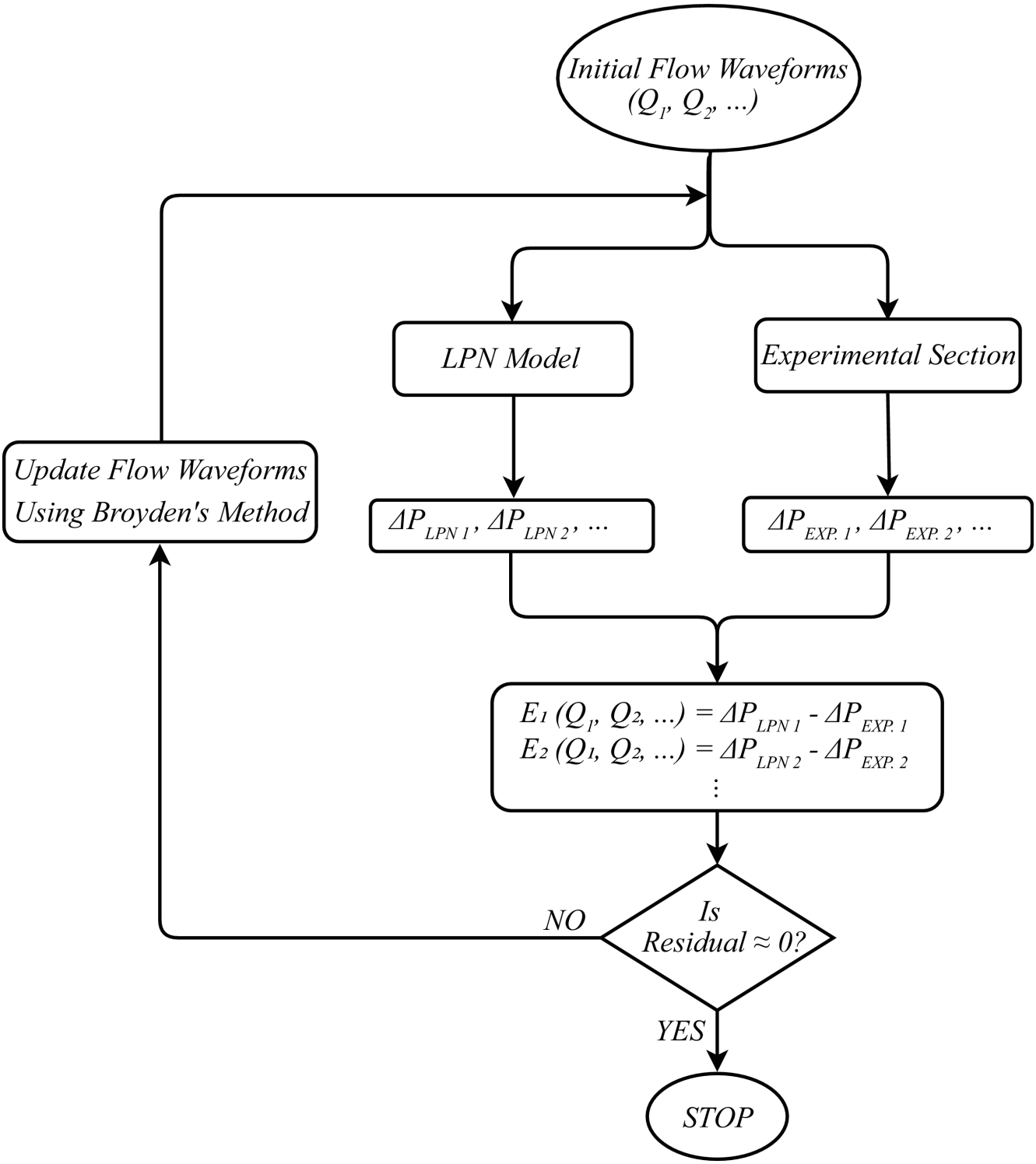

Ehsan Mirzaei

Figure 3. Illustration of coupling (A) 2, (B) 3 & (C) 4-branch virtual experiments to the venous side of a Fontan LPN

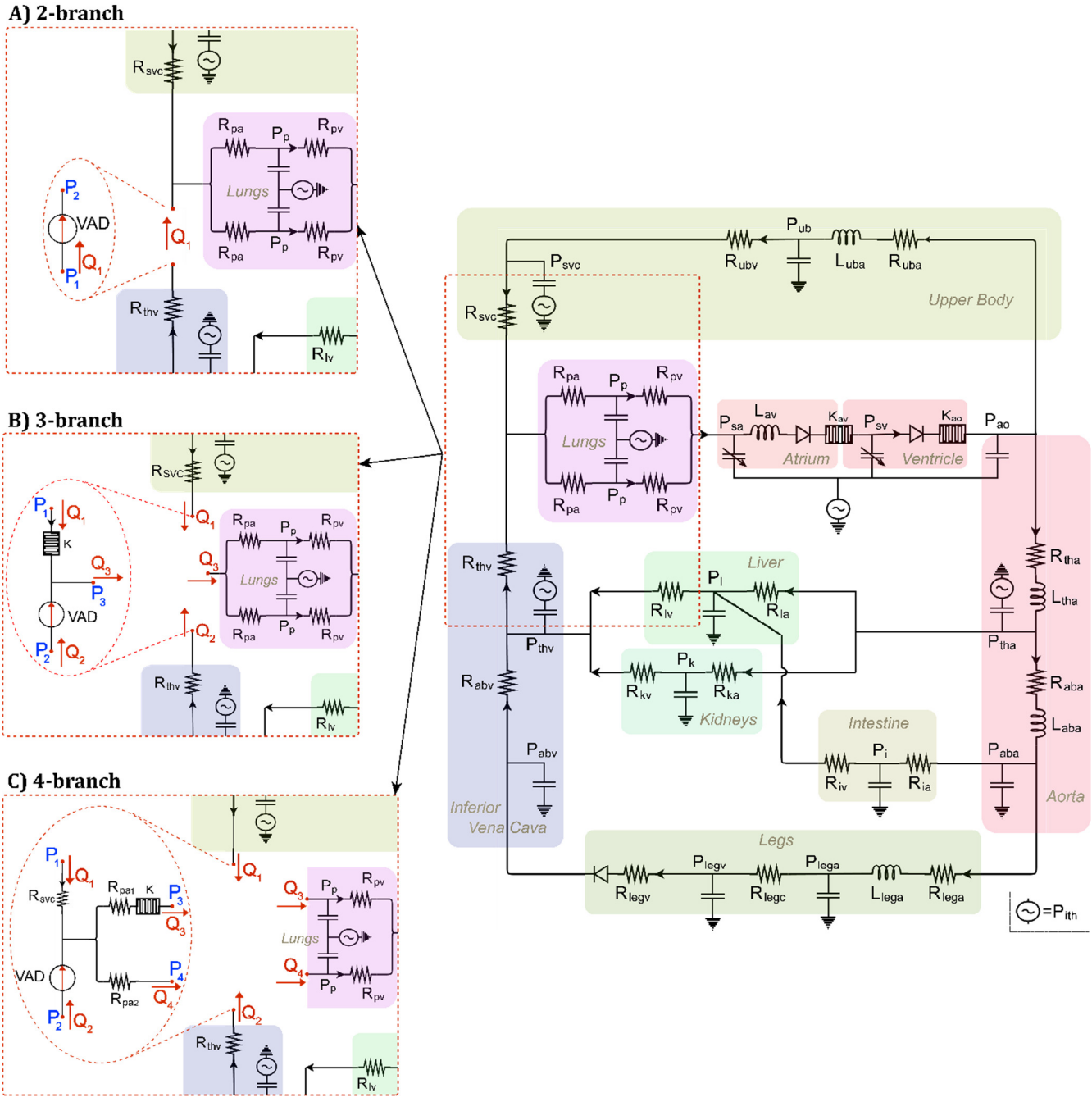

Ehsan Mirzaei

Figure 4. Illustration of coupling (**A**) 2 & (**B**) 3-branch virtual experiments to the arterial side of a Fontan LPN

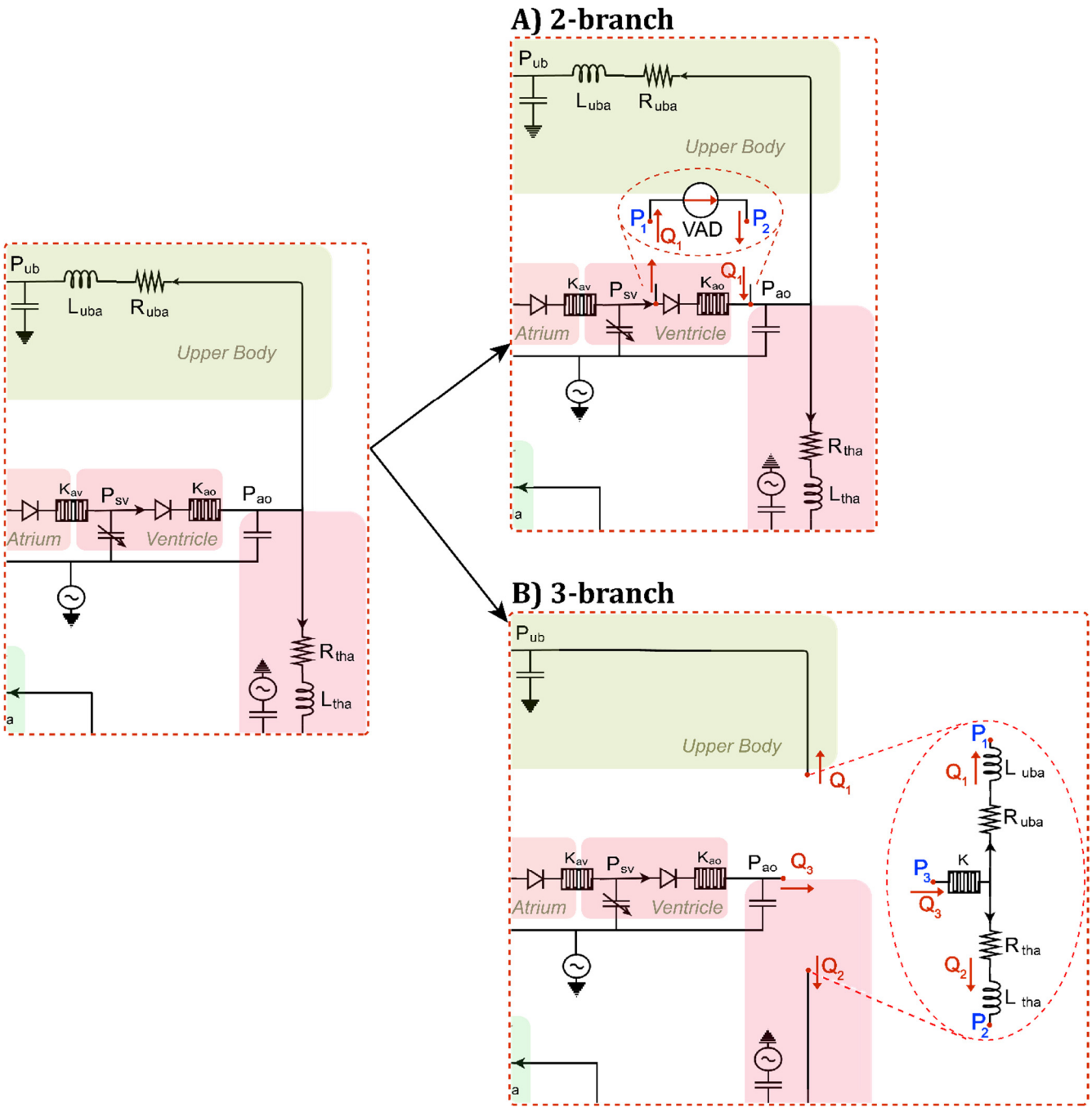

Masoud Farahmand

Figure 5. Demonstration of coupling algorithm applied to a physical experiment. (**A**) A stenosis model is coupled to the IVC location of (**B**) a numerical model of Fontan circulation. (**C**) A hydraulic flow experiment operates the stenosis model.

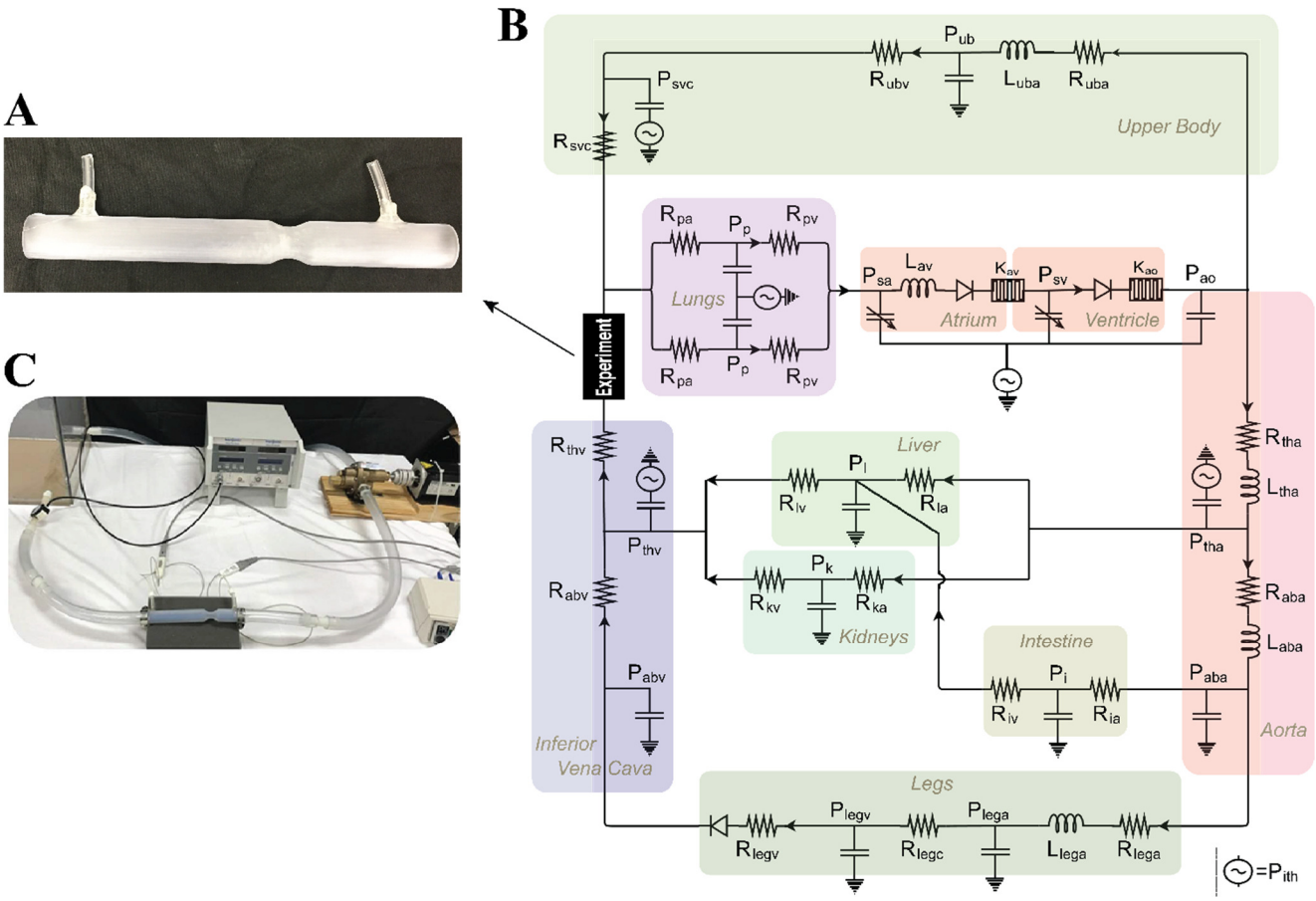

Masoud Farahmand

Figure 6. Schematic of the physical experiment setup.

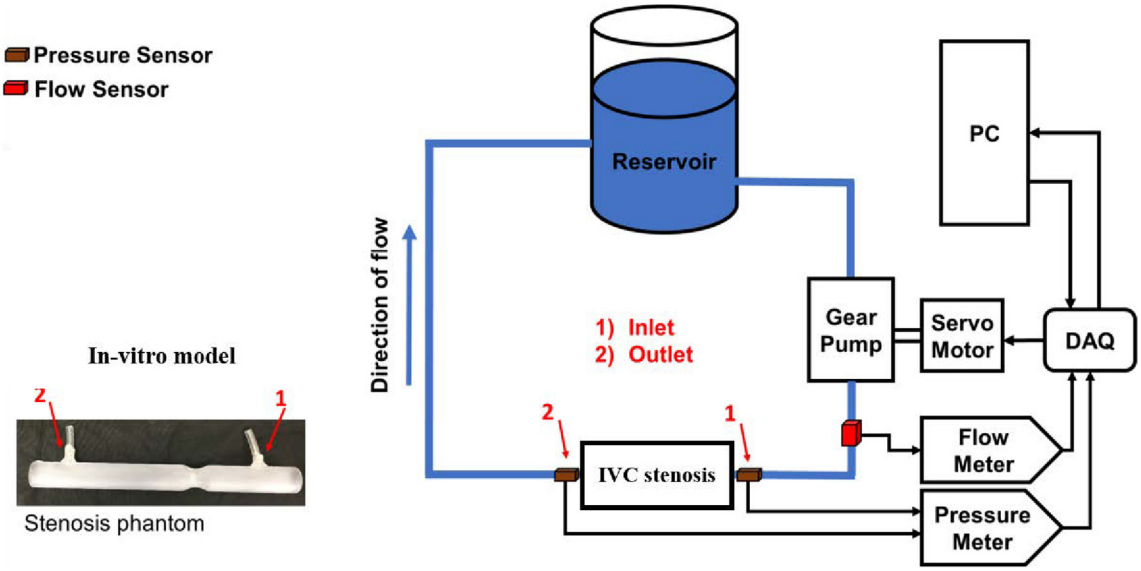

Ehsan Mirzaei

Figure 7. Comparisons of the flow and pressure waveform solutions from the coupling algorithm for (A) 2, (B) 3 & (C) 4-branch venous side coupling against the true solutions

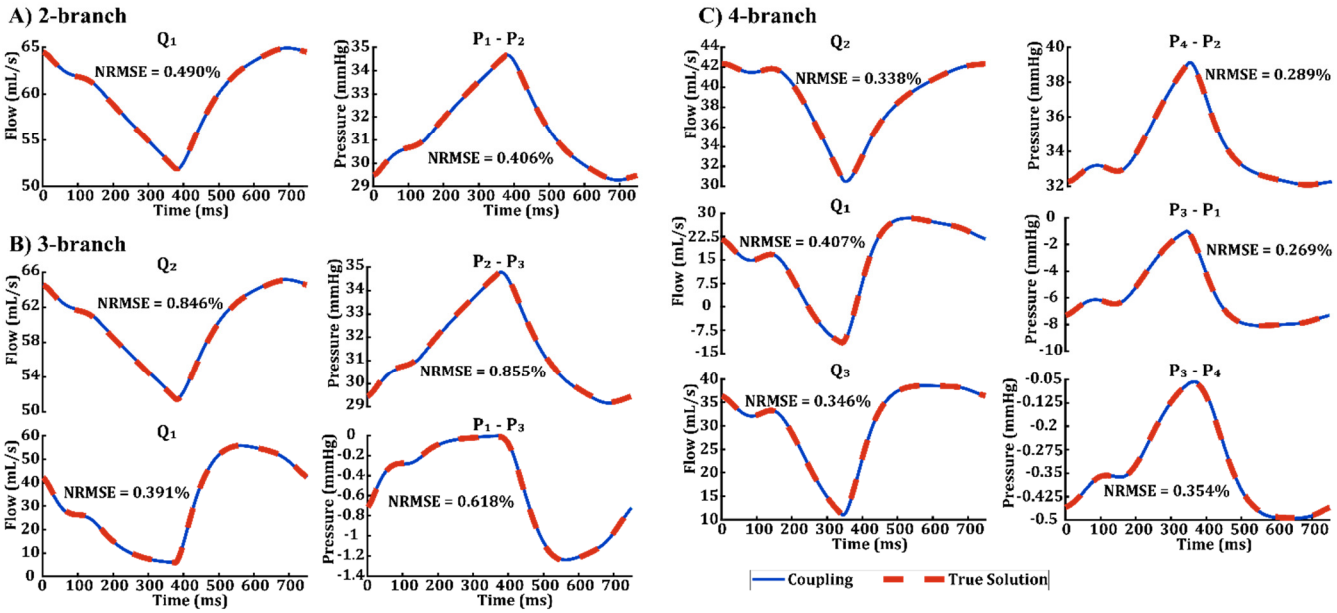

Ehsan Mirzaei

Figure 8. Comparisons of the flow and pressure waveform solutions from the coupling algorithm for (A) 2 & (B) 3-branch arterial side coupling against the true solutions

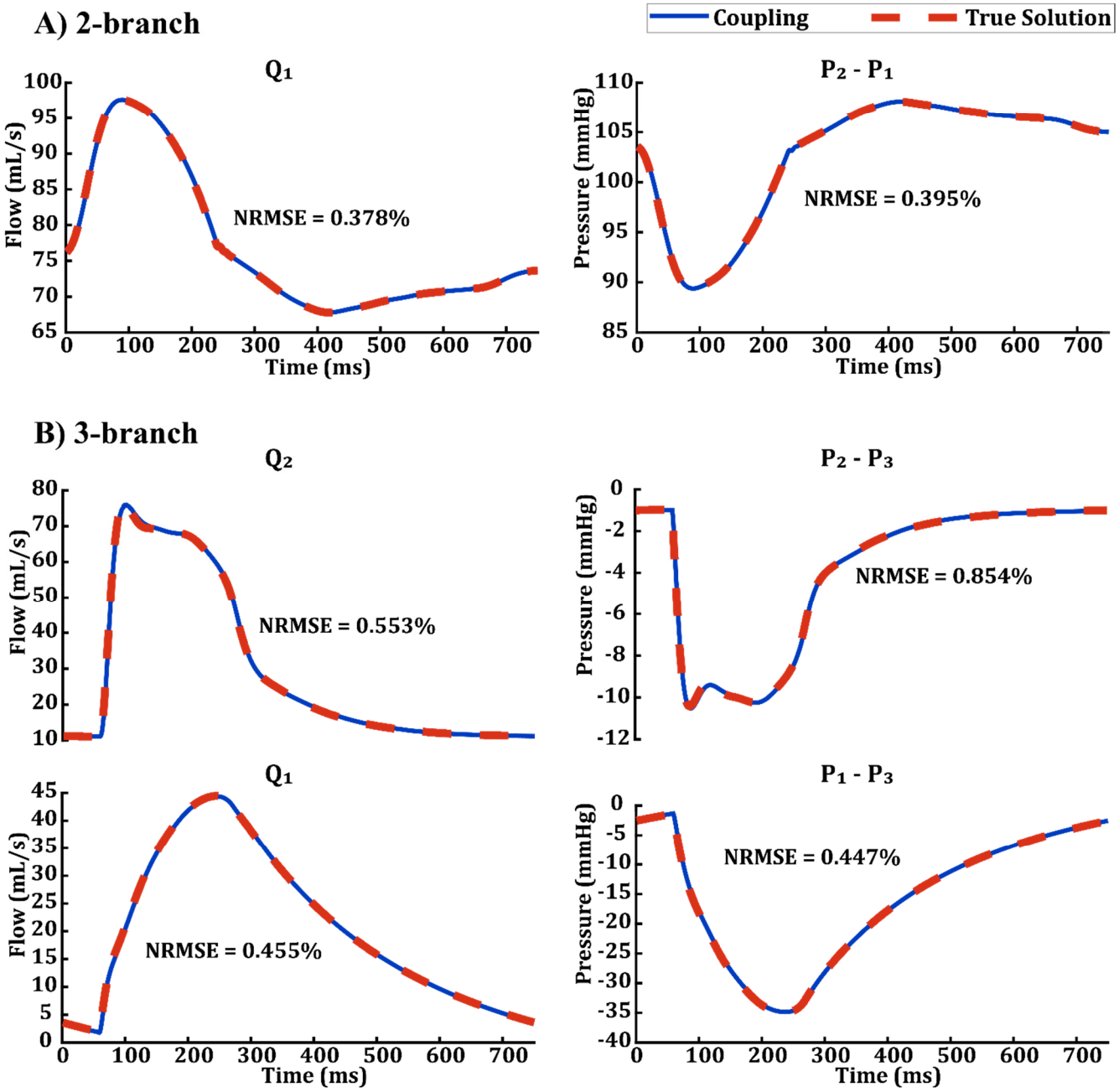

Ehsan Mirzaei

Figure 9. Comparisons of residual decrease rates between two branches of the 3-branch coupling on both (A) venous and (B) arterial sides and the corresponding pressure changes

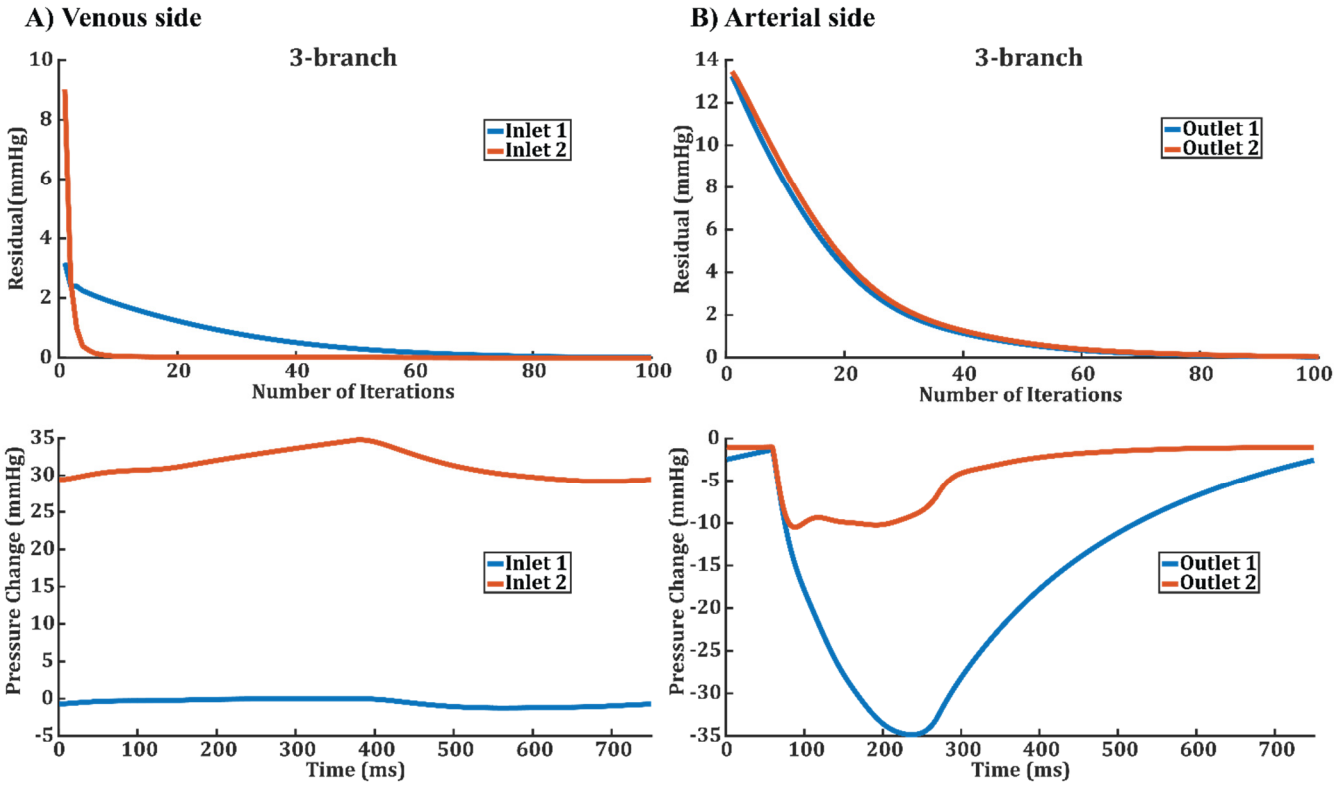

Masoud Farahmand

Figure 10. Results of coupling a physical flow experiment containing an 85% IVC stenosis with the closed loop LPN. (**A**) The flow solution of the final (30^{th}) iteration revealed the effect of the IVC stenosis on the IVC flow (**B**) the residual successfully achieved the convergence criterion of 0.04 mmHg after 30 iterations.